Measurement of Homonuclear Proton Couplings Based on Cross-Peak Nulling in CT-COSY

Zhengrong Wu and Ad Bax

Laboratory of Chemical Physics, National Institute of Diabetes and Digestive and Kidney Diseases, National Institutes of Health, Bethesda, Maryland 20892

A method in which ^1H–^1H scalar and dipolar couplings are obtained from the cross-peak nulling condition in a series of constant-time (CT) COSY spectra, as a function of the duration of the CT period, is described. The method is best suited for measurement of ^1H–^1H couplings in the range 5–20 Hz. It is shown, however, that results can be sensitive to cross-correlated relaxation effects. Also, artifactual resonances, resulting from strong coupling, can be quite pronounced in CT-COSY spectra, even when $|J_{AB}/(\delta_A - \delta_B)| < 0.1$. The experiments are demonstrated for the DNA dodecamer $d(\text{CGCGAATTCGCG})_2$, both in isotropic solution and in a liquid crystalline phase.

INTRODUCTION

The utility of ^1H–^1H J couplings in structure determination has long been recognized, and numerous methods for measuring these couplings in the case of overlapping multiplets have been proposed. These include homonuclear J-spectroscopy ([1]), homonuclear E.COSY methods ([2]), triple-resonance E.COSY techniques ([3]), quantitative J correlation ([4, 5]), comparison of cross sections through in-phase and antiphase cross peaks ([6, 7]), and the so-called DISCO method ([8]), which relies on the same principle.

Tunable, very weak degrees of molecular alignment with the magnetic field can be induced by dissolving the molecule of interest in a dilute liquid crystalline phase ([9]). Such liquid crystal media typically consist of oriented large particles, such as bicelles ([10]), filamentous phage ([11, 12]), or cellulose crystallites ([13]). Several other lyotropic liquid crystals also have been found suitable for this purpose ([14–16]). The partially aligned molecules permit measurement of internuclear dipolar couplings, which normally average to 0 in isotropic solution. ^1H–^1H dipolar couplings contain information on both the interproton distance and on the orientation of the interproton vector with respect to the molecular alignment tensor. However, quantitative measurement of ^1H–^1H coupling in the aligned state can become more complicated because the complexity of the ^1H multiplet greatly increases due to a multitude of unresolvable splittings. For ^{15}N-labeled proteins, homonuclear dipolar couplings involving $^1H^N$ can be measured with the HNHA experiment ([9, 17]), and were shown to improve structural quality

([18, 19]). For ^{13}C-labeled proteins, an interesting method for measuring methylene ^1H–^1H couplings has been developed ([20]). Recently, it has been demonstrated that the CT-COSY experiment ([21]) can be used for measurement of ^1H–^1H dipolar couplings in oligosaccharides and proteins, without the requirement of heteronuclear labeling ([22, 23]). This type of measurement relies on the nonlinearity of the CT-COSY cross peak to diagonal peak intensity ratio buildup as a function of the constant-time duration.

Here, we describe a different way of extracting ^1H–^1H couplings from CT-COSY spectra, which relies on the idea that all cross peaks from a proton, A, to protons other than X change sign when the constant-time duration, CT, crosses the $CT = (2N + 1)/(2J_{AX})$ condition ($N = 0, 1, \ldots$). The method is demonstrated for an unlabeled oligonucleotide, $d(\text{CGCGAATTCGCG})_2$, which recently has been studied in detail using heteronuclear dipolar couplings, combined with very qualitative ^1H–^1H couplings, estimated from cross-peak intensities in a regular COSY spectrum ([24]).

We find that the CT-COSY experiment can yield remarkably intense artifactual cross peaks that result from non-first-order effects (strong coupling), even if the difference in chemical shift is rather large, $|\delta_A - \delta_B| > 10|J_{AB}|$. A method to attenuate such artifacts is also described.

It is well recognized that in macromolecules, cross-correlated relaxation ([25]) can affect the measurement of ^1H–^1H couplings considerably. From the deoxyribose structure, the cross peaks that are expected to have a cross correlation contribution are easily predicted. Analysis of the remaining cross peaks is shown to yield accurate measurements for the corresponding ^1H–^1H couplings.

MATERIALS AND METHODS

The unlabeled DNA dodecamer, $d(\text{CGCGAATTCGCG})_2$, was purchased from Midland Certified Reagent Company (Midland, TX). It was dialyzed against sterilized H_2O using a 2500-MW cutoff dialysis cassette and subsequently lyophilized to dryness. The powder was then dissolved in D_2O buffer, containing 10 mM sodium phosphate (pH 6.8), 50 mM KCl, and 0.02% sodium azide. Two different NMR samples were used for
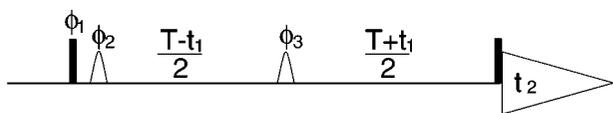
FIG. 1. Pulse scheme of the 2D CT-COSY experiment. Rectangular pulses correspond to 90° flip angles. The two shaped pulses are of the hyperbolic secant type (26), and have durations of 500 μs each. Phase cycling: $\phi_1 = y$; $\phi_2 = x$; $\phi_3 = x, y, -x, -y$; Receiver $= x, -x$. Quadrature detection in the t_1 dimension is accomplished by simultaneously incrementing ϕ_1, ϕ_2, and ϕ_3 in the regular States–TPPI manner.

measuring ^{1}H–^{1}H couplings at DNA concentrations of approximately 2 mM duplex, one isotropic sample and one liquid crystalline sample, based on use of the filamentous phage Pf1 (12). The liquid crystal sample contained 20 mg/ml Pf1 phage (ASLA Labs, http://130.237.129.141//asla/asla-phage.htm), which was first exchanged into the same D_2O buffer as mentioned above by using a 30-kD cutoff centricon concentrator. All measurements were carried out in 300-μl Shigemi microcells at 35°C. Experiments were performed on a Bruker DRX-800 spectrometer, equipped with a triple-resonance, three-axis pulsed field gradient probehead.

CT-COSY spectra were recorded with the pulse scheme of Fig. 1. A hyperbolic secant-shaped 180° inversion pulse was used to ensure perfect inversion (26), together with a second such pulse just after the first 90° ^{1}H pulse, which refocuses the effect of F_1 phase distortion introduced by the (moving) 180° pulse (27). Spectra were acquired with the maximum number of t_1 increments, except for cases where CT > 50 ms, where the t_1 time domain was truncated at 50 ms. The t_2 acquisition time was 63.9 ms. Spectral widths were 8 kHz in both t_1 and t_2, and 4–16 transients were acquired per complex t_1 increment, resulting in total measuring times of 1–4 h per spectrum.

The data were processed using the program NMRPipe (28). In the t_2 dimension, the data were apodized with a squared cosine bell window, followed by zero filling to 2048. In the t_1 dimension, for spectra with less than 50-ms constant-time t_1 evolution periods, mirror-image linear prediction (29) was used to extend the time domain to 50 ms, followed by apodization with a 72°-shifted sine bell window and zero filling to 2048 data points.

RESULTS AND DISCUSSION

Ignoring cross-correlated transverse relaxation, and assuming the weak coupling limit, the time domain signals of the A-spin diagonal, $S_{AA}(t_1, t_2)$, and AX cross peak, $S_{AX}(t_1, t_2)$, in a CT-COSY experiment are given by

$$S_{AA}(t_1, t_2) = S_o \Pi_k \cos(\pi J_{Ak}T) \cos(\Omega_A t_1) \exp(-T/T_{2A})$$

$$\times \Pi_k \cos(\pi J_{Ak}t_2) \exp(i\Omega_A t_2) \exp(-t_2/T_{2A}) \quad [1a]$$

$$S_{AX}(t_1, t_2) = S_o \sin(\pi J_{AX}T) \Pi_{k \neq X} \cos(\pi J_{Ak}T) \cos(\Omega_A t_1)$$

$$\times \exp(-T/T_{2A}) \sin(\pi J_{AX}t_2) \Pi_{q \neq A} \cos(\pi J_{X_q}t_2)$$

$$\times \exp(i\Omega_X t_2) \exp(-t_2/T_{2X}), \quad [1b]$$

where the products extend over all spins k coupled to A, and spins q coupled to X, T is the duration of the constant-time evolution period, S_o is the diagonal time domain signal strength for $T = t_2 = 0$, Ω_A and Ω_X are angular chemical shifts of spins A and X, and T_{2A} and T_{2X} are the A- and X-spin transverse relaxation times. In the weakly coupled limit, the effects of scalar and dipolar couplings are additive, and J_{PQ} here refers to the sum of the scalar and dipolar couplings between spins P and Q.

After 2D Fourier transformation, the S_{AX}/S_{AA} intensity ratio is proportional to $\tan(\pi J_{AX}T)$, although the proportionality constant is a complex function of the X-spin multiplet shape and is generally unknown. As shown by Tian *et al.* (22), J_{AX} can be derived from this ratio provided at least two CT-COSY spectra are recorded, where for at least one of the two $J_{AX}T > \sim 0.5$, so that $\tan(\pi J_{AX}T)$ becomes nonlinear in J_{AX}. For unlabeled macromolecules, the diagonal resonance is frequently not resolvable, and in the present study we simply focus on the cross-peak signal of Eq. [1b]. As can be seen from this expression, the AX cross-peak intensity is proportional to $\Pi_{k \neq X} \cos(\pi J_{Ak}T)$, so it reaches a null when $J_{Ak}T = \frac{1}{2}$, and changes sign when comparing spectra recorded with $J_{Ak}T < \frac{1}{2}$ and $\frac{1}{2} < J_{Ak}T < \frac{3}{2}$. Because the same passive coupling typically modulates several cross peaks, multiple measurements for a single coupling are typically obtained from a series of CT-COSY spectra recorded with different T values. In essence, the J value is obtained from intensity nulling of cross peaks, and we refer to the method as JINX.

A limitation of JINX is that if large couplings are present, the shortest T value should preferably be smaller than $(2J_{max})^{-1}$. If a single passive coupling is larger than $(2T)^{-1}$, all cross peaks involving this passive coupling will have opposite sign relative to cross peaks between spins that do not involve large passive couplings. Accurate fitting of the cross-peak intensity modulation as a function of T can be difficult in such cases. A second, related problem is that for short values of T, the inherent resolution in the t_1 dimension of the 2D spectra is poor. To some extent this can be remedied by mirror-image linear prediction of the nondecaying t_1 time domain data (29), although this adversely affects the accuracy of cross-peak intensities. Thirdly, only the absolute value of the coupling is obtained, which in the case of dipolar couplings can present problems during structure calculation (19).

Effects of Strong Coupling on CT-COSY Spectra

Extra resonance lines are observed in 2D homonuclear J-spectra of non-first-order spin systems. Their origin is easily understood by considering that the eigenfunctions in such systems are no longer simple products of the wave function of the individual spins, but linear combinations thereof (30–32). Non-first-order effects can also give rise to artifactual cross peaks in heteronuclear correlation and NOESY spectra (33, 34). The reason for the extra complexity occurring in the 2D CT-COSY is similar to that in the 2D J-spectrum, and below we briefly

discuss the effects of non-first-order coupling on CT-COSY spectra. As we will show, these effects can be remarkably large.

In the case of two spins, A and B, with a scalar coupling J_{AB} and a dipolar coupling D_{AB}, the Hamiltonian under free precession is described by

$$\mathbf{H}_o = \delta_A I_{Az} + \delta_B I_{Bz} + (J_{AB} + D_{AB})I_{Az}I_{Bz}$$
$$+ (J_{AB} - \tfrac{1}{2}D_{AB})(I_{Ax}I_{Bx} + I_{Ay}I_{By}), \qquad [2]$$

where δ_A and δ_B are the resonance frequencies of spins A and B. Fully analogous to the textbook case of an AB scalar-coupled spin system, the stationary eigenfunctions of the system are linear combinations of the wave functions of the individual spins (35)

$$\Psi_1 = |\alpha\alpha\rangle \qquad [3a]$$
$$\Psi_2 = \cos\theta|\alpha\beta\rangle + \sin\theta|\beta\alpha\rangle \qquad [3b]$$
$$\Psi_3 = \cos\theta|\beta\alpha\rangle - \sin\theta|\alpha\beta\rangle \qquad [3c]$$
$$\Psi_4 = |\beta\beta\rangle \qquad [3d]$$

with their energies

$$E_1 = -\tfrac{1}{2}(\delta_A + \delta_B) + \tfrac{1}{4}(J_{AB} + D_{AB}) \qquad [4a]$$
$$E_2 = -\tfrac{1}{2}\big[(\delta_B - \delta_A)^2 + \big(J_{AB} - \tfrac{1}{2}D_{AB}\big)^2\big]^{1/2}$$
$$- \tfrac{1}{4}(J_{AB} + D_{AB}) \qquad [4b]$$
$$E_3 = \tfrac{1}{2}\big[(\delta_A - \delta_B)^2 + \big(J_{AB} - \tfrac{1}{2}D_{AB}\big)^2\big]^{1/2}$$
$$- \tfrac{1}{4}(J_{AB} + D_{AB}) \qquad [4c]$$
$$E_4 = +\tfrac{1}{2}(\delta_A + \delta_B) + \tfrac{1}{4}(J_{AB} + D_{AB}), \qquad [4d]$$

where θ is a measure for the non-first-order character of the coupling defined as

$$\theta = \tfrac{1}{2}\arctan\big\{\big(J_{AB} - \tfrac{1}{2}D_{AB}\big)/(\delta_A - \delta_B)\big\}. \qquad [4e]$$

Below we will focus on the case where the non-first-order effect is relatively small ($\theta \ll 1$), such that the frequencies of the A-spin doublet to a good approximation equal $\delta_A \pm (J_{AB} + D_{AB})/2$. A perfect $180°$ pulse converts the mixed states into linear combination of stationary eigenstates:

$$\Psi'_1 = |\beta\beta\rangle = \Psi_4 \qquad [5a]$$
$$\Psi'_2 = \cos\theta|\beta\alpha\rangle + \sin\theta|\alpha\beta\rangle = \sin 2\theta\,\Psi_2 + \cos 2\theta\,\Psi_3 \qquad [5b]$$
$$\Psi'_3 = \cos\theta|\alpha\beta\rangle - \sin\theta|\beta\alpha\rangle = \cos 2\theta\,\Psi_2 - \sin 2\theta\,\Psi_3 \qquad [5c]$$
$$\Psi'_4 = |\alpha\alpha\rangle = \Psi_1. \qquad [5d]$$

For convenience, we will refer to coherences between Ψ_1 and Ψ_2 and between Ψ_3 and Ψ_4 as B-spin transitions, even while

they contain a small fraction of A-spin coherence. These two coherences, σ_{12} and σ_{34}, have frequencies defined by $E_1 - E_2$, and $E_3 - E_4$, respectively, i.e., approximately $\delta_B \pm \tfrac{1}{2}(J_{AB} + D_{AB})$. After a $180°$ pulse, the coherences are redistributed according to

$$\sigma_{12} \rightarrow \sin 2\theta\,\sigma_{24} + \cos 2\theta\,\sigma_{34} \qquad [6a]$$
$$\sigma_{34} \rightarrow -\sin 2\theta\,\sigma_{13} + \cos 2\theta\,\sigma_{12} \qquad [6b]$$

and similar equations for the A-spin coherences. This process is schematically shown in Fig. 2. Doublet components of B are rotated by $180°$ about y, but are attenuated by $\cos\theta$, and a $\sin\theta$ fraction is transferred into spin A magnetization, with the 1–3 component antiphase with respect to 1–2. The relative intensities of the two B-spin doublet components retain their regular $(1 + \sin 2\theta)/(1 - \sin 2\theta)$ ratio, and the same for the newly formed A-spin magnetization. This latter magnetization contributes to the anomalous cross peak. Just prior to the final $90°$ pulse, the angles α_{13} and α_{24} in Fig. 2C are given by

$$\alpha_{13} = -\omega_{34}(T/2 - t_1/2) + \omega_{13}(T/2 + t_1/2) + \pi$$
$$= (\omega_{13} - \omega_{34})T/2 + \tfrac{1}{2}(\omega_{13} + \omega_{34})t_1 + \pi \qquad [7a]$$
$$\alpha_{24} = -\omega_{12}(T/2 - t_1/2) + \omega_{24}(T/2 + t_1/2)$$
$$= (\omega_{24} - \omega_{12})T/2 + \tfrac{1}{2}(\omega_{24} + \omega_{12})t_1. \qquad [7b]$$

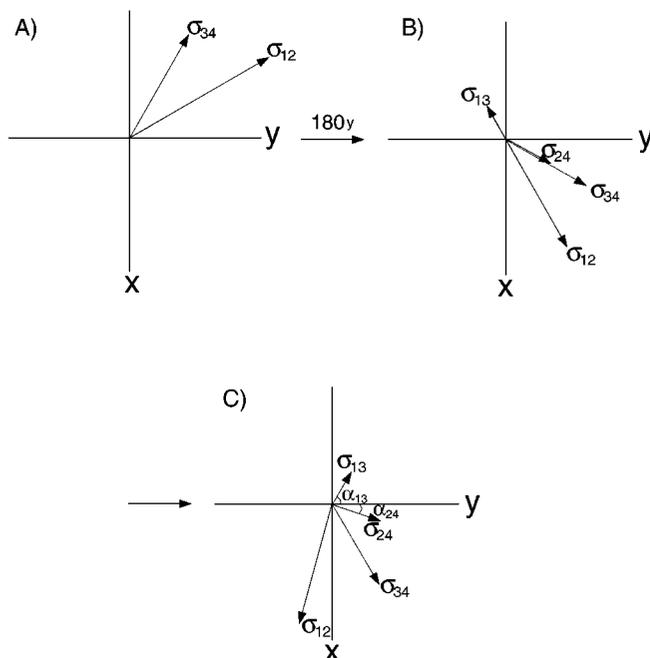**FIG. 2.** Evolution of coherences σ_{12} and σ_{34} during the CT-COSY experiment. (A) Just prior to the moving $180°$ pulse; (B) just after the $180°$ pulse, when part of the σ_{12} and σ_{34} coherences has been transferred to σ_{24} and σ_{13}; (C) immediately prior to the final $90°$ pulse.

The phase of both of these "spurious" vectors is modulated by $\frac{1}{2}(\omega_{24} + \omega_{12}) = \frac{1}{2}(\omega_{13} + \omega_{34}) = (\Omega_A + \Omega_B)/2$, where Ω_A and Ω_B are the angular chemical shifts of spins A and B, respectively. The difference in phase is $\alpha_{13} - \alpha_{24} = \pi + 2\pi J_{AB}T$, so, for T durations where the regular doublet components are antiphase, this spurious A-spin magnetization, which originated from the B-spin doublet, is in-phase just prior to the final 90° pulse and gives rise to an in-phase F_2 A-spin doublet, as shown in Fig. 3A. This in-phase doublet is of maximum intensity for a T duration that maximizes A–B cross-peak intensity. In contrast, when $T = N/J_{AB}$, i.e., when regular cross peaks are the weakest (Fig. 3C), the spurious antiphase B-spin magnetization is transferred back to A by the mixing pulse, yielding an antiphase A-spin signal in F_2. Figure 3B shows the artifactual resonances when $1/J_{AB} < T < 3/2J_{AB}$, in which case they are the superposition of in-phase and antiphase components in the F_2 dimension.

In the F_1 dimension, the A–B artifact at $F_1 = (\Omega_A + \Omega_B)/4\pi$ is a singlet with a phase that rapidly oscillates as a function of T, with a frequency equal to half the A–B chemical shift difference (cf. Eqs. [7a], [7b]). Note that the intensity ratio of the spurious to regular peaks is on the order of $\tan(2\theta)$, and even for a case of weak coupling, where $(\Omega_A - \Omega_B)/2\pi = 10 \times J_{AB}$ as in Fig. 3A, the spurious cross peak intensities are 10% of the maximum achievable regular cross-peak intensity (for $T = 3/2J_{AB}$). For the case where $T \approx 1/J_{AB}$ (Fig. 3C) the regular cross peaks are very weak, and the artifacts become stronger than the A–B cross peaks.

ABX Spin System

As discussed below, for ABX spin systems, the strong-coupling induced artifacts in CT-COSY spectra can be as strong or stronger than the true A–X and B–X cross peaks. The same simple vector analysis, described above for the AB system, can be used, provided we assume $|J_{AX} + J_{BX} - D_{AX}/2 - D_{BX}/2| \ll |\Omega_A - \Omega_B|/2\pi$. The A-spin originating magnetization, transferred to B by the 180° pulse in the manner described above, yields a cross-peak contribution to X, centered at $(F_1, F_2) = [(\Omega_A + \Omega_B)/4\pi, \Omega_X/2\pi]$. At $t_1 = 0$, the signal contributing to this spurious cross peak has an amplitude proportional to $\tan(2\theta)\, \sin[\pi(J_{AX} + J_{BX} + D_{AX} + D_{BX})T/2]\sin[\pi(J_{AB} + D_{AB})T]$, and an F_1 phase of $(\Omega_B - \Omega_A)T/2$. This $A \rightarrow B \rightarrow X$ artifactual cross peak superimposes on the $B \rightarrow A \rightarrow X$ cross peak, which has the same amplitude, but an F_1 phase of $(\Omega_A - \Omega_B)T/2$. The first component is antiphase with respect to B in the F_2 dimension, the $B \rightarrow A \rightarrow X$ cross peak is antiphase with respect to A. Nevertheless, the two cross peaks can constructively interfere, particularly when $J_{AX} + D_{AX} \approx J_{BX} + D_{BX}$, and yield a cross peak with an intensity of up to $2\tan(2\theta)$ for $(J_{AB} + D_{AB})T = (2N + 1)/2$. Note that for this duration of T the regular AX and BX cross peaks have vanishing intensity (Eq. [1b]). In addition to this main contribution to this artifactual cross peak, there is a second contribution that is $\sin(2\theta)$ weaker, and de-
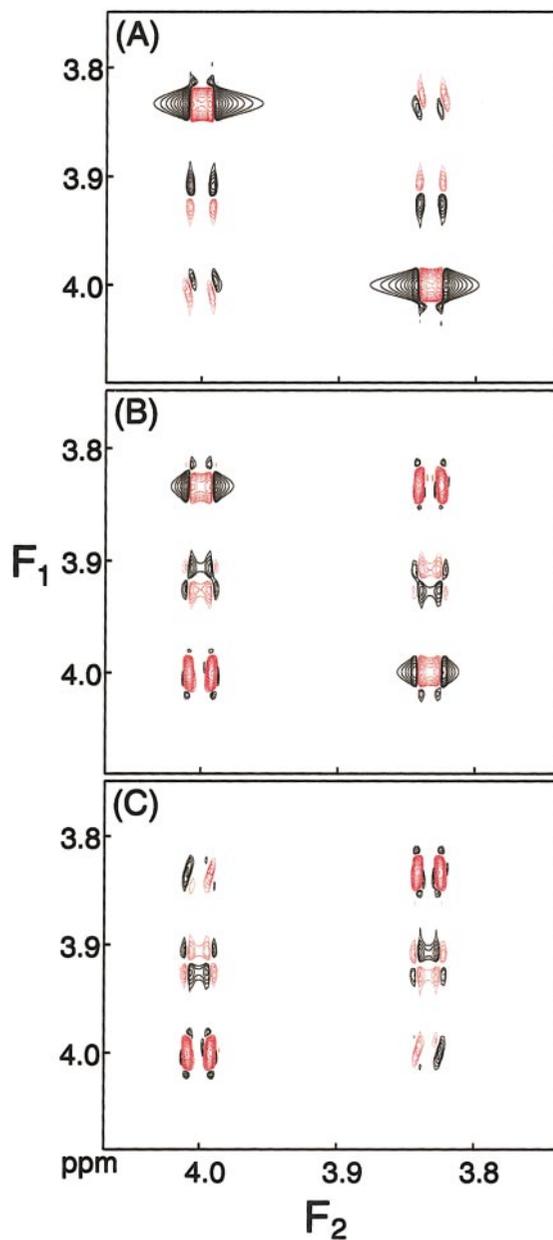

FIG. 3. Simulated 2D CT-COSY spectra, showing the artifactual resonances between two strongly coupled spins A and B, which have a chemical shift difference $\delta = 100$ Hz and scalar coupling $J_{AB} = 10$ Hz, at different constant-time delays of (A) 150, (B) 110, and (C) 100 ms.

pends on $\cos[\pi(J_{AX} + J_{BX} + D_{AX} + D_{BX})T/2]\cos[\pi(J_{AB} + D_{AB})T]$. These contributions are calculated under the condition of relatively weak coupling ($|J_{AB}| < \sim 5|\Omega_A - \Omega_B|/2\pi$), but show fair agreement with results from simulations with the ANTIOPE program (*36*) and the Bruker NMRSIM spectral simulation program, which take the strong coupling effects into account rigorously.

The $A \rightarrow B \rightarrow X$ and $B \rightarrow A \rightarrow X$ pathways yield artifactual cross-peak contributions that have opposite F_1 phase dependencies on the duration T. A simple way to attenuate these artifacts
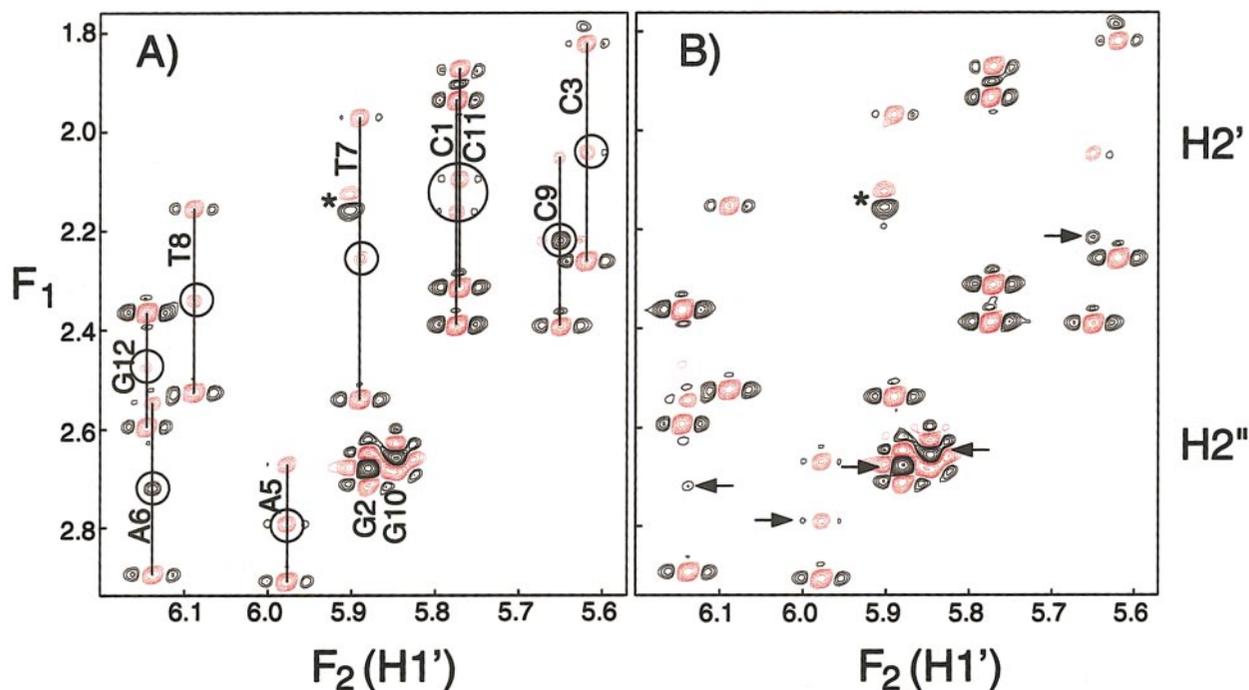
FIG. 6. H1′–H2′/H2″ regions of the 800-MHz CT-COSY spectra of d(CGCGAATTCGCG)$_2$, (A) recorded with a constant-time duration, T, of 37.5 ms, and (B) obtained by co-addition of CT-COSY spectra recorded with $T = 35.5, 36.5, 37.5, 38.5,$ and 39.5 ms. Black and red contours correspond to positive and negative intensity, respectively. The artifactual resonances caused by strong coupling are circled in (A) (except for G2 and G10, where H2′ and H2″ nearly overlap). The arrows indicate the attenuated but not completely eliminated artifactual resonances for A5, A6, and C9, and virtually unchanged artifacts for G2 and G10. The resonance marked by an asterisk originated from a small molecule impurity in the sample. The spectra have been phased such that the diagonal is absorptive, and the antiphase cross peaks are dispersive in F_2 but absorptive in the constant-time F_1 dimension. Owing to their antiphase nature, the dispersive cross peaks actually have the appearance of resolution-enhanced absorptive signals, with net zero integral.

simply coadds two spectra collected for T-durations that differ by $2\pi/(\Omega_A - \Omega_B)$.

Cross-Correlated Relaxation

When extracting the size of J and dipolar couplings from cross-peak intensities in CT-COSY spectra, it is important to take into account the effects of cross-correlated relaxation (25, 37, 38). As described in detail by Wimperis and Bodenhausen (25), the presence of cross-correlated relaxation can give rise to significant antiphase magnetization terms after a period of free evolution. As a result, cross peaks can appear in COSY spectra, even in the absence of J coupling (39, 40). Analogously, in the application of CT-COSY to the measurement of J couplings in DNA, the interference between cross-correlated relaxation and J-dephasing can alter the duration of the constant-time, T, for which nulling of a cross peak occurs.

For a simple three-spin AMX system that is relaxed solely by the AX, AM, and MX dipolar interactions, the different relaxation rates of the four A-spin multiplet components can easily be understood by considering the dipolar field at spin A caused by different spin states of the M and X spins. If A, M, and X are arranged linearly, the dipolar fields of spin X and M at the site of spin A will add up if they are parallel

($MX = |\alpha\alpha\rangle$ or $|\beta\beta\rangle$), but partially cancel each other if they are anti-parallel ($MX = |\alpha\beta\rangle$ or $|\beta\alpha\rangle$). Consequently, the multiplet components of spin A that experience the stronger local field ($MX = |\alpha\alpha\rangle$ or $|\beta\beta\rangle$) will relax faster than those corresponding to $MX = |\alpha\beta\rangle$ or $|\beta\alpha\rangle$. After the initial $90°_y$ pulse in the CT-COSY experiment, the transverse magnetization of spin A can be written as

$$A_x = (A_x + 4A_xM_zX_z)/2 + (A_x - 4A_xM_zX_z)/2, \quad [8]$$

where the $(A_x + 4A_xM_zX_z)$ term corresponds to the two fast-relaxing multiplet components of spin A, and the second term corresponds to the two slower relaxing components. If Γ and Γ_{cc} are the auto- and cross-correlated relaxation rates, and $G^{\pm} = \exp[-T(\Gamma \pm \Gamma_{cc})]$, the transverse magnetization of on-resonance spin A at time T after an initial $90°_y$ pulse is described by

$$
\begin{aligned}
A_x \rightarrow \tfrac{1}{2}G^+ \{ &\cos[\pi(J_{AM} + J_{AX})T](A_x + 4A_xM_zX_z) \\
+ &\sin[\pi(J_{AM} + J_{AX})T](2A_yM_z + 2A_yX_z) \} \\
+ \tfrac{1}{2}G^- \{ &\cos[\pi(J_{AM} - J_{AX})T](A_x - 4A_xM_zX_z) \\
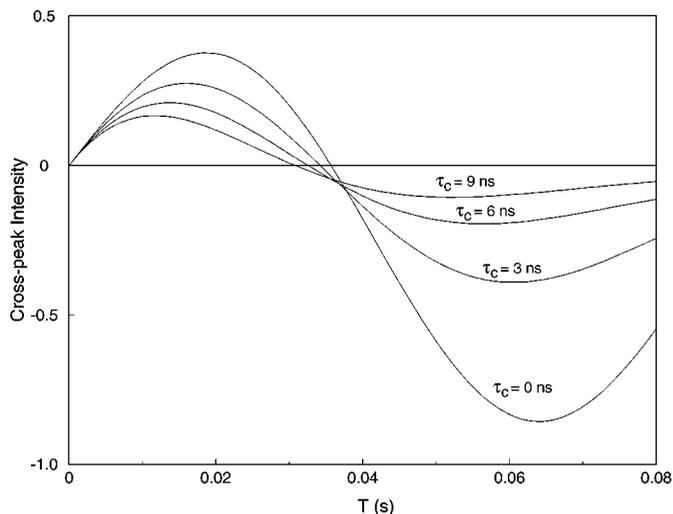+ &\sin[\pi(J_{AM} - J_{AX})T](2A_yM_z - 2A_yX_z) \}. \quad [9]
\end{aligned}
$$

FIG. 4. Calculated $A \rightarrow M$ cross-peak intensity in an AMX spin system as a function of the constant-time duration for τ_c of 0, 3, 6, and 9 ns. The AMX spin system simulates the H1′–H2″–H2′ spin system in a deoxyribose with the geometry shown in Fig. 8. The following coupling values were used: $J_{AM} = 10$ Hz; $J_{AX} = 14$ Hz. The effect of dipole–dipole auto- and cross-correlated T_2 relaxation is taken into account, but the finite lifetime of spin X is ignored to exemplify the effect of cross-correlated relaxation on the JINX condition.

The terms $2A_y M_z$ in Eq. [9] give rise to the AM cross peak after the subsequent 90° mixing pulse. If $G^+ = G^- = G$, the cross-peak intensity is simply proportional to $\frac{1}{2}G\{\sin[\pi(J_{AM} + J_{AX})T] + \sin[\pi(J_{AM} - J_{AX})T]\} = G\sin(\pi J_{AM}T)\cos(\pi J_{AX}T)$, and nulling of the cross-peak intensity occurs when $T = (N + \frac{1}{2})/J_{AX}$. However, when $G^+ \neq G^-$, this nulling condition is shifted. Figure 4 shows numerical examples of how much the nulling condition in a typical AMX system may be affected for different values of the rotational correlation time, τ_c. In the example shown, the constant-time duration at which a nulling condition of the AM cross peak occurs is reduced with increasing correlation time, resulting in overestimation of J_{AX}.

The dipole–dipole cross-correlation rate, Γ_{cc}, depends on the angle, θ_{AMAX}, between the AM and AX internuclear vectors (25):

$$\Gamma_{cc} \propto r_{AM}^{-3} r_{AX}^{-3}(3\cos^2\theta_{AMAX} - 1), \quad [10]$$

where r_{AM} and r_{AX} are the internuclear distances. As can be seen from Eq. [10], when θ_{AMAX} approaches the "magic angle" of 54.7°, Γ_{cc} reduces to 0. As we will show for deoxyribose, by selecting spin-pair interactions that as a result of this angular dependence are inherently less sensitive to cross correlation, reliable values for the H2′–H2″ couplings can be measured.

The change in apparent coupling caused by cross correlation depends on the values of the couplings involved. The dipolar coupling in a liquid crystalline medium can be substantially larger than the J coupling itself, and the apparent change in coupling caused by cross-correlated relaxation therefore can

be quite different in the isotropic and liquid crystalline states, so it is important to note that the cross-correlated relaxation effect does not cancel out when calculating the dipolar couplings from the difference in apparent coupling in the two states.

Passive Spin Relaxation

As emphasized by Harbison, the finite lifetime of the passive spin reduces the apparent splitting of an in-phase doublet relative to the true J coupling (41). This effect also is important when analyzing a range of other J coupling measurements, including HNHA (4, 42, 43) and J-modulated HMQC (42, 43). Figure 5 shows how much JINX-derived J couplings are affected by passive spin relaxation, as a function of the selective T_1 of the passively coupled spin. Clearly, as is the case for the other experiments mentioned above, the effect is largest for small couplings and becomes small when the coupling is much larger than the inverse of the selective T_1 of the passive spin.

Application to DNA

The analyses described above are illustrated for the double-stranded B-DNA dodecamer, d(CGCGAATTCGCG)$_2$. With a chemical shift difference between H2′ and H2″ of 200–500 Hz (at 800 MHz) and $J_{H2'H2''} \approx 14$ Hz, the H1′–H2′–H2″ spin system would normally be considered as a first-order AMX-type spin system. However, as can be seen in Fig. 6A, rather intense artifactual resonances can appear midway between the H2″–H1′ and H2′–H1′ cross peaks, whose intensities are in quantitative agreement with values predicted on the basis of non-first-order effects discussed above. As mentioned under *ABX Spin*
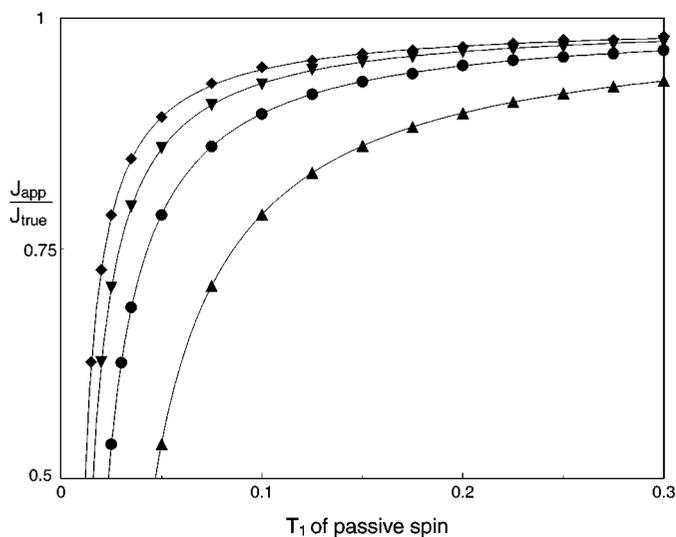

FIG. 5. The ratio of the apparent J_{AX} coupling (J_{app}) over the true coupling (J_{true}) derived using JINX of the $A \rightarrow M$ cross peak in an AMX spin system, as a function of the T_1 of spin X. The J_{app}/J_{true} ratio is calculated for J_{true} values of 5 (▲), 10 (●), 15 (▼), and 20 Hz (◆), assuming $T_2^A = 100$ ms, $T_1^M = 200$ ms, and $J_{AM} = 4$ Hz.

System, these cross peaks can be attenuated by coaddition of spectra recorded over a narrow range of constant-time durations. Figure 6B corresponds to the sum of five such spectra, collected with T durations spaced 1 ms apart, and centered around $T = 37.5$ ms. Most of the artifactual peaks encircled in Fig. 6A are eliminated in Fig. 6B. However, the intense artifacts for the quite strongly coupled G2 and G10 sugars remain because the difference in H2′ and H2″ chemical shift frequency is small compared to the changes in T durations used. Similarly, the A5, A6, and C9 artifacts are merely attenuated and not eliminated because no single set of five different T durations can achieve complete elimination of these artifacts for all deoxyribose sugars in the dodecamer simultaneously.

Figure 7 shows the fit of the H2′–H2″, H2′–H1′, and H2″–H3′ cross-peak intensities for nucleotide C3, as a function of T, to Eq. [1b]. Each set of five closely spaced points, recorded for the artifact suppression described above, shows a smooth T dependence of the intensity changes and a virtual absence of scatter in these high S/N data. As will be discussed in more detail below, the first null in the H2′–H3′ curve (caused by the passive H2′–H2″ couplings) is affected by H2′–H3′ dipolar cross correlation with H2′–H2″, and occurs slightly earlier than the null in the H2′–H1′ curve. This H2′–H1′ curve is nearly free of cross correlation (see below), and the first T duration with zero intensity is close to $1/(2J_{H2'H2''})$. The second zero crossing in the H2′–H3′ curve occurs when the $\cos(\pi J_{H2'H1'} T)$ term in Eq. [1b] reaches zero, and coincides with the first null of the H2′–H2″ curve, yielding two independent measurements for $J_{H2'H1'}$.

Figure 8 shows a deoxyribose sugar ring with a typical B-DNA 2′-endo conformation. Considering a three-spin system H1′–H2′–H2″, the dipole–dipole cross-correlated relaxation rate, Γ_{CC} (cf. Eq. [10]), between H2″–H1′ and H2″–H2′ is relatively large because the H1′–H2″–H2′ angle is approximately 90°. As a re-
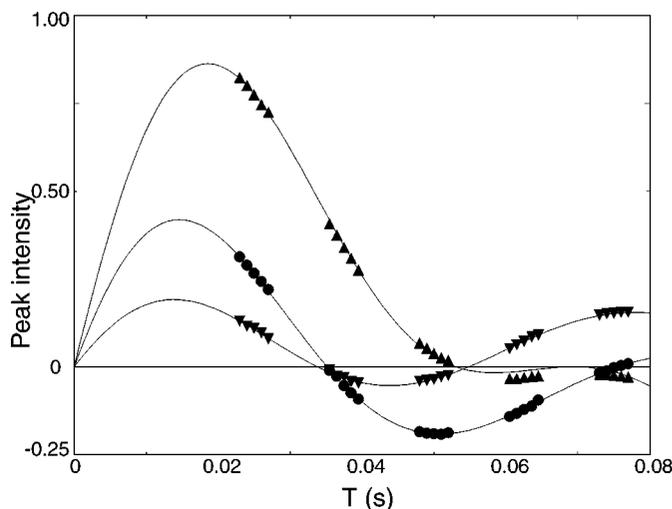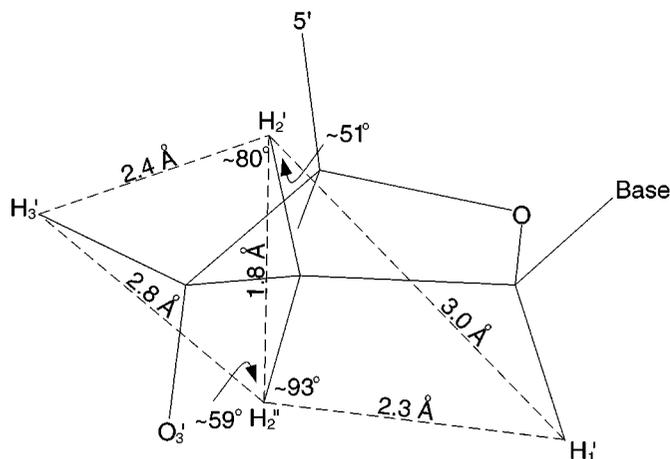

FIG. 8. Interproton distances and angles in a typical B-DNA 2′-endo deoxyribose sugar.

sult, the H2″–H1′ cross peak cannot be used for accurate measurement of $J_{H2'H2''}$, and neither can the H2″–H2′ cross peak be used for measuring $J_{H1'H2''}$. Throughout, an A–B cross peak refers to a cross peak at the frequency of spin A in the F_1 dimension and spin B in F_2. Interestingly, the H1′–H2′–H2″ angle is close to the magic angle of 54.7°, where cross correlation equals 0 (Eq. [10]). Consequently, $J_{H2'H2''}$ can be determined by monitoring at what T value the H2′–H1′ cross peak changes sign (Eq. [1b]). Similarly, in the case of H2′–H2″–H3′, $J_{H2'H2''}$ can be determined from the H2″–H3′ cross peak, but not from the H2′–H3′ cross peak.

The above features are illustrated in Fig. 9, for four sections taken from the CT-COSY spectra of the Dickerson dodecamer. Durations of the constant-time evolution period range from 23 to 64.5 ms, and each spectrum actually represents the sum of five 2D spectra, with T durations 1 ms apart, and centered at $T = 25, 37.5, 50,$ and 62.5 ms.

The cross peaks in the H1′ region of the spectrum are labeled in Fig. 9A, with the upfield F_1 signals corresponding to H2′–H1′ interactions and the downfield ones to H2″–H1′. When the constant-time duration is increased from 25 ms (Fig. 9A) to 37.5 ms (Fig. 9B), the H2′–H1′, H2″–H1′, and H2′–H3′ cross peaks all change signs, but not the H2′–H2″ cross peaks, indicating that $J_{H2'H2''}$ is the largest coupling. Figures 9E and 9F are F_2 cross sections through H2′ of C3 in Figs. 9A and 9B. Although both H2′–H1′ and H2′–H3′ cross peaks change signs between $T = 25$ ms and $T = 37.5$ ms, interpolation of the nulling condition for the H2′–H1′ cross peak yields $J_{H2'H2''} = 14.2$ Hz, whereas a slightly larger value of 14.8 Hz is obtained if the nulling condition of the H2′–H3′ were used to derive $J_{H2'H2''}$. As mentioned above, cross-correlated relaxation between the H3′–H2′ and H2″–H2′ dipolar interactions shifts the nulling condition for this cross peak, whereas for the H2′–H1′ this effect is expected to be very small. Similarly, if the nulling condition were derived from the H2″–H1′ cross peak ($T_{null} = 31$ ms) the

FIG. 7. Fit of the H2′–H2″ (▲), H2′–H1′ (●), and H2′–H3′ (▼) cross-peak intensities for nucleotide C3 to Eq. [1b], as a function of the constant-time duration, T.
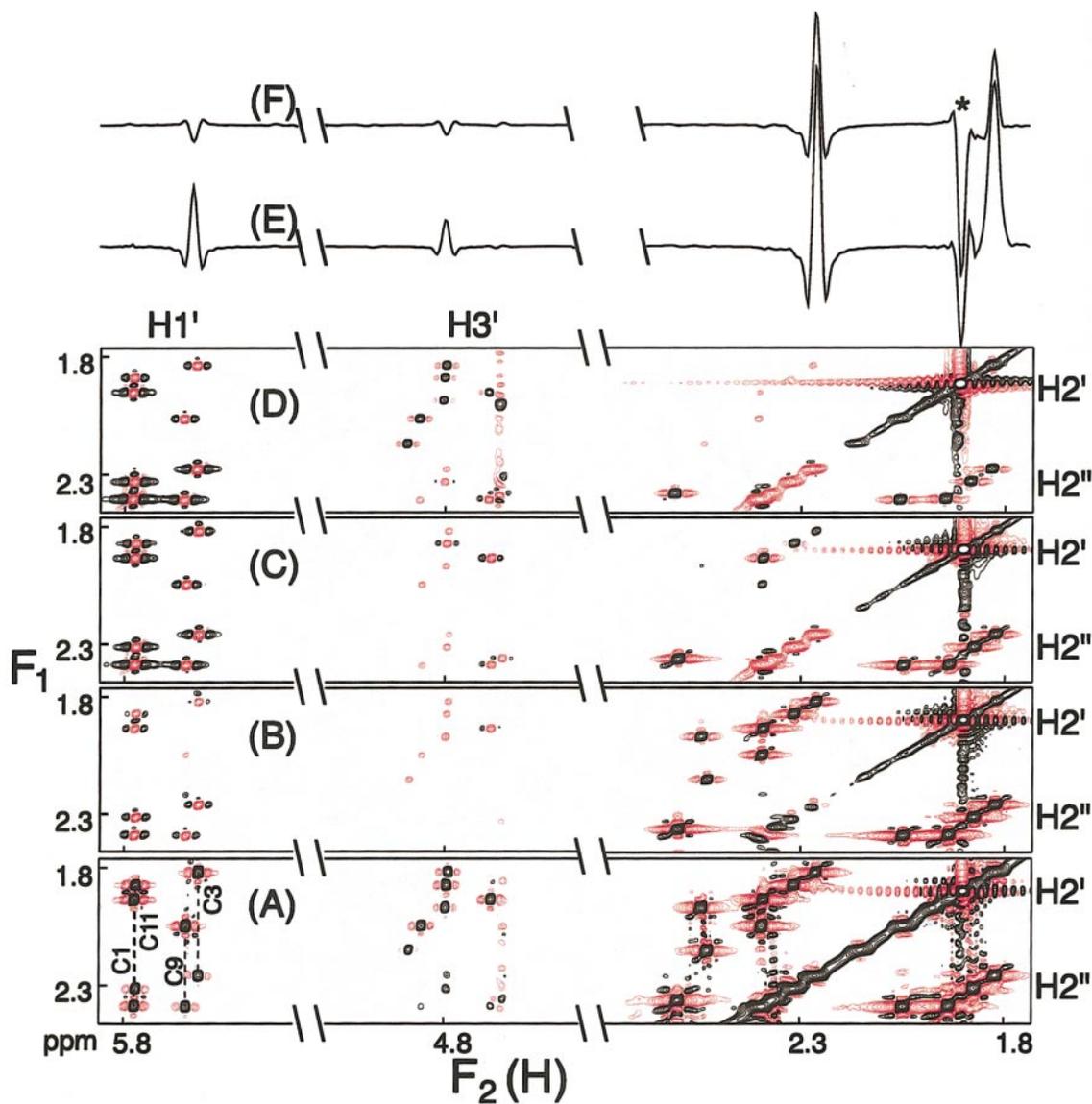
FIG. 9. Small region from a series of 800-MHz CT-COSY spectra for d(CGCGAATTCGCG)$_2$. Spectra are obtained by co-addition of five CT-COSY data sets, recorded with CT durations of (A) 23–27, (B) 35.5–39.5, (C) 48–52, and (D) 60.5–64.5 ms. (E) F_2 cross section through spectrum (A) at the C3–H2$'$ frequency; and (F) the same cross section from spectrum (B). The H1$'$–H2$'$/H2$''$ peaks are labeled in spectrum (A). The asterisk in (F) marks the signal from a small molecule impurity in the sample.

stronger cross-correlation effect yields an even larger apparent $J_{H2'H2''}$ coupling of 16.2 Hz.

When increasing the constant-time duration from 50 ms (Fig. 9C) to 62.5 ms (Fig. 9D) both the H2$'$–H3$'$ and H2$'$–H2$''$ cross peaks change signs, but the H2$'$–H1$'$ cross peak does not. This indicates that $J_{H1'H2'}T$ has become larger than $\frac{1}{2}$, with the precise values for $J_{H1'H2'}$ again determined by interpolation. Table 1 lists the ^{1}H–^{1}H coupling constants measured for the DNA dodecamer measured using this method. These values are in close agreement with those reported previously from P.E.COSY measurements (44), and recently remeasured using selective deuteration (45).

DNA in Phage Medium

Figure 10 shows small portions of CT-COSY spectra recorded for $T = 25$, 35, and 45 ms for the Dickerson dodecamer in 20 mg/ml Pf1 phage. Additional cross peaks between H2$'$ and the aromatic protons, not present in isotropic solution, are seen in the left-hand region of these panels. These mark through-space dipolar couplings, which on average tend to be smaller than couplings (sum of $J + D$) between H2$'$ and other sugar protons. Cross peaks between H2$'$ and H3$'$ are particularly strong compared to the spectrum of Fig. 9, suggesting that $D_{H2'H3'}$ has the same sign as $J_{H2'H3'}$, i.e., positive. This is confirmed by

TABLE 1
Isotropic ^{1}H–^{1}H J Couplings in d(CGCGAATTCGCG)$_2$

Nucleotide	$J_{2'2''}$	$J_{1'2'}$	$J_{1'2''}$	$J_{2'3'}$
C1	14.3[a]	8.5[a]/8.2[b]/7.9[c]	6.3[a]/6.1[b]/6.2[c]	5.9[a]/6.3[b]/—[c]
G2	14.4	11.1/10.1/9.7	5.5/5.7/5.8	5.4/—/4.5
C3	14.2	9.1/8.8/8.9	6.2/6.2/5.8	6.6/6.1/—
G4	13.5	11.0/10.2/10.0	6.0/5.1/5.6	5.5/—/—
A5	14.0	9.7/9.7/9.8	6.1/5.7/6.5	5.4/—/5.1
A6	14.2	9.3/9.3/9.5	5.7/6.0/6.2	5.4/—/5.1
T7	14.5	9.1/8.3/8.6	6.4/6.2/6.6	7.1/—/—
T8	14.6	9.8/9.5/9.8	6.3/6.0/6.5	6.0/—/5.7
C9	13.7	9.2/8.7/8.9	6.0/6.0/5.6	6.5/6.3/5.6
G10	14.3	11.2/9.7/9.9	5.7/5.5/6.0	5.4/—/—
C11	14.3	8.8/8.4/8.3	6.2/6.2/6.3	6.6/6.6/—
G12	14.7	7.8/8.1/7.8	6.7/6.3/6.3	6.0/6.3/—

[a] Measured by the CT-COSY method.
[b] Previously measured using P.E.COSY (*44*).
[c] Average of previous measurements by Yang *et al* (*45*).

spectra recorded at lower phage concentration (7 mg/ml, data not shown), which show a small increase in H2′–H3′ cross-peak intensity, thereby excluding the possibility that $D_{H2'H3'}$ and $J_{H2'H3'}$ have opposite signs.

For residues C1, C3, T7, and C11, the H2′–H1′ and H2′–aromatic cross peaks either change signs or become vanishingly weak when T is increased from 25 to 35 ms (Figs. 10A, B),

which confirms the large (13–17 Hz) values for $J_{H2'H3'} + D_{H2'H3'}$, in good agreement with a structure recently calculated on the basis of primarily heteronuclear one-bond dipolar interactions and qualitative ^{1}H–^{1}H couplings (24). Interestingly, as can be seen in Fig. 10B, for C9 the H2′–H1′ and H2′–G10H8 cross peaks stay positive when increasing T from 25 to 35 ms, whereas both the H2′–H3′ and H2′–H2″ cross peaks change signs. This is caused by a change in sign of both the $\cos[\pi(J_{H2'H2''} + D_{H2'H2''})T]$ and the $\cos[\pi(J_{H2'H3'} + D_{H2'H3'})T]$ terms in Eq. [1b]. As both terms are present for the H2′/H1′ and H2′/G10H8 interaction, but only one for the H2′–H3′ and H2′–H2″ cross peaks, only these latter two change signs. Remarkably, C9 is the only nucleotide for which $J_{H2'H2''} + D_{H2'H2''}$ increases with phage concentration; for all others $J_{H2'H2''}$ and $D_{H2'H2''}$ have opposite signs. At 20 mg/ml Pf1 phage we found, for example, that for C9 $|J_{H2'H2''} + D_{H2'H2''}| = 17 \pm 1$ Hz, whereas for C3 $|J_{H2'H2''} + D_{H2'H2''}|$ is less than 5 Hz. Considering that the geminal J coupling is quite similar for all sugars in this dodecamer (Table 1), the large variations in $|J_{H2'H2''} + D_{H2'H2''}|$ are attributed to variations in $D_{H2'H2''}$; i.e., they are caused by different orientations of the H2′–H2″ vector relative to the molecular alignment tensor.

The strong-coupling artifacts, highlighted in Fig. 6A, have below threshold intensity in Fig. 10. Although for most sugars in the phage medium the absolute value of $J_{H2'H2''} + D_{H2'H2''}$ is decreased relative to isotropic conditions, the degree of "strong
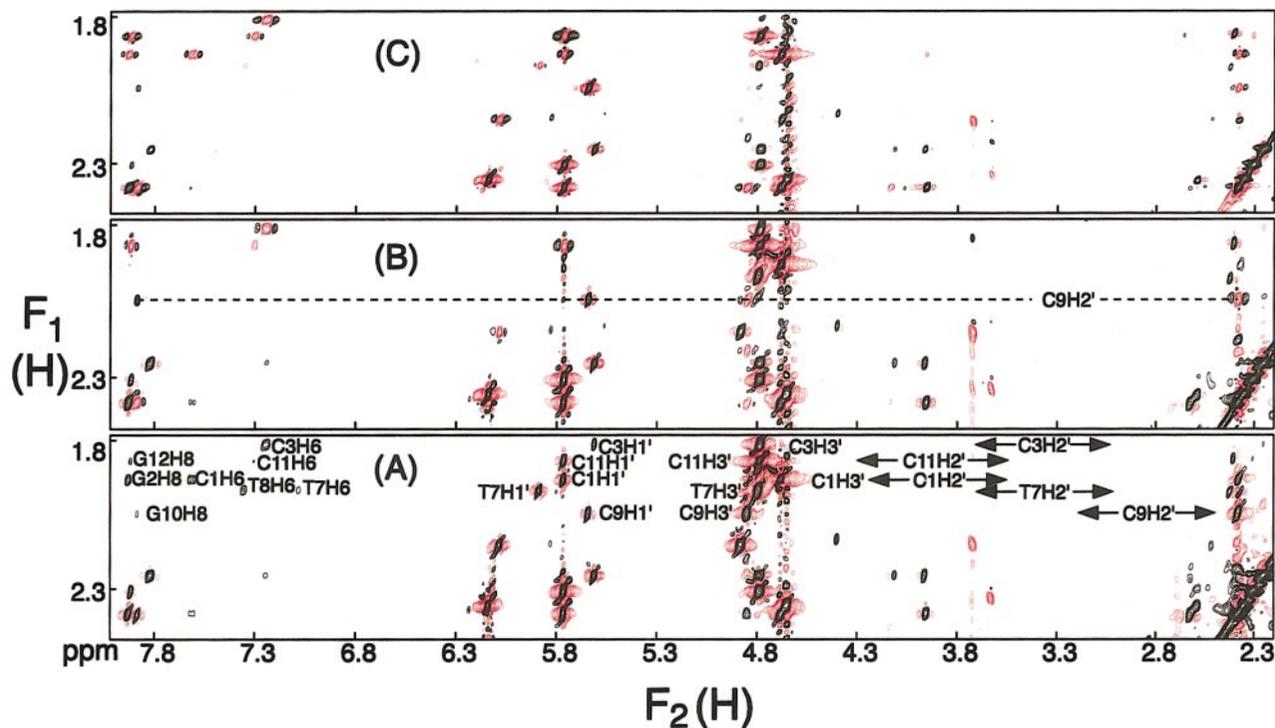

FIG. 10. Small regions of the 800-MHz CT-COSY spectra of d(CGCGAATTCGCG)$_2$ in 20 mg/ml Pf1, recorded with constant-time durations of (A) 25, (B) 35, and (C) 45 ms. Cross peaks from C9H2′, T7H2′, C1H2′, C11H2′, and C3H2′ to H3′, H1′, and base protons are labeled in (A).

coupling" as expressed by θ in Eq. [4e] actually depends on $(J_{AB} - \frac{1}{2}D_{AB})/(\delta_A - \delta_B)$, and therefore increases when J and D have opposite signs. However, as discussed under *ABX Spin System*, the artifact intensity also depends on $\sin[\pi(J_{AX} + J_{BX} + D_{AX} + D_{BX})T/2] \sin[\pi(J_{AB} + D_{AB})T]$ and both terms in this product are considerably smaller in the aligned state than in the isotropic phase.

CONCLUDING REMARKS

The JINX approach for measurement of ^{1}H–^{1}H couplings described above is reasonably robust. Like E.COSY methods (*2*), and unlike the HNHA or HACAHB experiments (*4, 5*), JINX derives the $J + D$ value from the passive and not the active coupling contribution to a cross peak. As a result, multiple independent measurements frequently can be obtained for a given coupling. However, as a result of cross correlation, significant distortions in the derived couplings can occur in slowly tumbling macromolecules, in particular when the internuclear vectors corresponding to the active and passive coupling partners are nearly at right angles relative to one another. No comprehensive overview of the sensitivity of other ^{1}H–^{1}H coupling measurement methods on cross-correlated relaxation has been published, and it therefore is unclear whether JINX is particularly sensitive to these effects or whether this is a common problem.

JINX is less appropriate for measurement of small ^{1}H–^{1}H couplings, particularly in macromolecules. For small couplings, a long constant-time duration is needed for the JINX condition, and the effect of the finite lifetime of the passive spin becomes rather large and results in an underestimate of the true coupling. This is a general problem with all quantitative J correlation experiments (*46*), but is particularly relevant for couplings involving ^{1}H in macromolecules, which as a result of rapid ^{1}H–^{1}H flip-flop interactions have short lifetimes for a given spin state.

The sign of the measured ^{1}H–^{1}H couplings is not directly available from JINX measurements. When the focus is on the measurement of ^{1}H–^{1}H dipolar couplings, the sign for geminal and vicinal ^{1}H–^{1}H interactions can usually be derived from measurement at two different nematogen concentrations. In this case, the sign for D_{HH} is simply derived from measurement under isotropic conditions and at two different concentrations of the liquid crystal, using the knowledge that the dipolar coupling scales approximately linearly with nematogen concentration. For ^{1}H–^{1}H pairs without a J coupling, the absolute value can be used in structure calculations (*19*). However, this results in up to twice the number of minima in the potential energy function during structure calculation. If a reasonably accurate structure can be calculated without these couplings, such a structure may be of sufficient quality to identify the sign of the dipolar couplings. Alternatively, E.COSY-like methods that permit experimental measurement of the sign of ^{1}H–^{1}H couplings have recently been described (*47, 48*).

REFERENCES

1. W. P. Aue, J. Karhan, and R. R. Ernst, Homonuclear broadband decoupling and two-dimensional J-resolved spectroscopy, *J. Chem. Phys.* **64,** 4226–4227 (1976).

2. C. Griesinger, O. W. Sørensen, and R. R. Ernst, Practical aspects of the E.COSY technique. Measurement of scalar spin-spin coupling constants in peptides, *J. Magn. Reson.* **75,** 474–492 (1987).

3. G. T. Montelione and G. Wagner, Accurate measurements of homonuclear HN-Ha coupling constants in polypeptides using heteronuclear 2D NMR experiments, *J. Am. Chem. Soc.* **111,** 5474–5475 (1989).

4. G. W. Vuister and A. Bax, Quantitative J correlation—A new approach for measuring homonuclear 3-bond J(HN-Ha) coupling-constants in 15N-enriched proteins, *J. Am. Chem. Soc.* **115,** 7772–7777 (1993).

5. S. Grzesiek, H. Kuboniwa, A. P. Hinck, and A. Bax, Multiple-quantum line narrowing for measurement of Ha-Hb J-couplings in isotopically enriched proteins, *J. Am. Chem. Soc.* **117,** 5312–5315 (1995).

6. J. J. Titman and J. Keeler, Measurement of homonuclear coupling-constants from NMR correlation spectra, *J. Magn. Reson.* **89,** 640–646 (1990).

7. T. Prasch, P. Groschke, and S. J. Glaser, SIAM, a novel NMR experiment for the determination of homonuclear coupling constants, *Angew. Chem.-Int. Edit.* **37,** 802–806 (1998).

8. H. Kessler, A. Muller, and H. Oschkinat, Differences and sums of traces within COSY spectra (disco) for the extraction of coupling-constants—Decoupling after the measurement, *Magn. Reson. Chem.* **23,** 844–852 (1985).

9. N. Tjandra and A. Bax, Direct measurement of distances and angles in biomolecules by NMR in a dilute liquid crystalline medium, *Science* **278,** 1111–1114 (1997).

10. C. R. Sanders and J. P. Schwonek, Characterization of magnetically orientable bilayers in mixtures of dihexanoylphosphatidylcholine and dimyristoylphosphatidylcholine by solid-state NMR, *Biochemistry* **31,** 8898–8905 (1992).

11. G. M. Clore, M. R. Starich, and A. M. Gronenborn, Measurement of residual dipolar couplings of macromolecules aligned in the nematic phase of a colloidal suspension of rod-shaped viruses, *J. Am. Chem. Soc.* **120,** 10,571–10,572 (1998).

12. M. R. Hansen, L. Mueller, and A. Pardi, Tunable alignment of macromolecules by filamentous phage yields dipolar coupling interactions, *Nat. Struct. Biol.* **5,** 1065–1074 (1998).

13. K. Fleming, D. Gray, S. Prasannan, and S. Matthews, Cellulose crystallites: A new and robust liquid crystalline medium for the measurement of residual dipolar couplings, *J. Am. Chem. Soc.* **122,** 5224–5225 (2000).

14. R. S. Prosser, J. A. Losonczi, and I. V. Shiyanovskaya, Use of a novel aqueous liquid crystalline medium for high-resolution NMR of macromolecules in solution, *J. Am. Chem. Soc.* **120,** 11,010–11,011 (1998).

15. L. G. Barrientos, C. Dolan, and A. M. Gronenborn, Characterization of surfactant liquid crystal phases suitable for molecular alignment and measurement of dipolar couplings, *J. Biomol. NMR* **16,** 329–337 (2000).

16. M. Ruckert and G. Otting, Alignment of biological macromolecules in novel nonionic liquid crystalline media for NMR experiments, *J. Am. Chem. Soc.* **122,** 7793–7797 (2000).

17. M. Pellecchia, C. W. Vander Kooi, K. Keliikuli, and E. R. P. Zuiderweg, Magnetization transfer via residual dipolar couplings: Application to

proton–proton correlations in partially aligned proteins, *J. Magn. Reson.* **143,** 435–439 (2000).

18. E. T. Olejniczak, R. P. Meadows, H. Wang, M. L. Cai, D. G. Nettesheim, and S. W. Fesik, Improved NMR structures of protein/ligand complexes using residual dipolar couplings, *J. Am. Chem. Soc.* **121,** 9249–9250 (1999).

19. N. Tjandra, J. Marquardt, and G. M. Clore, Direct refinement against proton–proton dipolar couplings in NMR structure determination of macromolecules, *J. Magn. Reson.* **142,** 393–396 (2000).

20. T. Carlomagno, W. Peti, and C. Griesinger, A new method for the simultaneous measurement of magnitude and sign of 1D(CH) and 1D(HH) dipolar couplings in methylene groups, *J. Biomol. NMR* **17,** 99–109 (2000).

21. A. Bax and R. Freeman, Investigation of complex networks of spin–spin coupling by two-dimensional NMR, *J. Magn. Reson.* **44,** 542–561 (1981).

22. F. Tian, P. J. Bolon, and J. H. Prestegard, Intensity-based measurement of homonuclear residual dipolar couplings from CT-COSY, *J. Am. Chem. Soc.* **121,** 7712–7713 (1999).

23. F. Tian, C. A. Fowler, E. R. Zartler, F. A. Jenney, M. W. Adams, and J. H. Prestegard, Direct measurement of H-1-H-1 dipolar couplings in proteins: A complement to traditional NOE measurements, *J. Biomol. NMR* **18,** 23–31 (2000).

24. N. Tjandra, S. Tate, A. Ono, M. Kainosho, and A. Bax, The NMR structure of a DNA dodecamer in an aqueous dilute liquid crystalline phase, *J. Am. Chem. Soc.* **122,** 6190–6200 (2000).

25. S. Wimperis and G. Bodenhausen, Relaxation-allowed cross-peaks in two-dimensional NMR correlation spectroscopy, *Mol. Phys.* **66,** 897–919 (1989).

26. M. S. Silver, R. I. Joseph, and D. I. Hoult, Selective population inversion in NMR, *Nature* **310,** 681–683 (1984).

27. S. Conolly, G. Glover, D. Nishimura, and A. Macovski, A reduced power selective adiabatic spin-echo pulse sequence, *Magn. Reson. Med.* **18,** 28–38 (1991).

28. F. Delaglio, S. Grzesiek, G. W. Vuister, G. Zhu, J. Pfeifer, and A. Bax, Nmrpipe—A multidimensional spectral processing system based on Unix pipes, *J. Biomol. NMR* **6,** 277–293 (1995).

29. G. Zhu and A. Bax, Improved linear prediction for truncated signals of known phase, *J. Magn. Reson.* **90,** 405–410 (1990).

30. G. Bodenhausen, R. Freeman, G. A. Morris, and D. L. Turner, NMR spectra of some simple spin systems studied by two-dimensional Fourier transformation of spin echoes, *J. Magn. Reson.* **31,** 75–95 (1978).

31. A. Kumar, Two-dimensional spin-echo NMR spectroscopy: A general method for calculation of spectra, *J. Magn. Reson.* **30,** 227–249 (1978).

32. A. Bax, "Two-Dimensional Nuclear Magnetic Resonance in Liquids," Reidel, Dordrecht (1982).

33. L. E. Kay and R. E. D. McClung, A product operator description of AB and ABX spin systems, *J. Magn. Reson.* **77,** 258–273 (1988).

34. V. V. Krishnan, S. Raghothama, and A. Kumar, Strong coupling and flip-angle dependence of coupling patterns in heteronuclear shift correlation two-dimensional NMR Spectra, *J. Magn. Reson.* **79,** 328–335 (1988).

35. E. D. Becker, "High Resolution NMR. Theory and Applications," Academic Press, San Diego (2000).

36. F. S. Debouregas and J. S. Waugh, Antiope, a program for computer experiments on spin dynamics, *J. Magn. Reson.* **96,** 280–289 (1992).

37. T. J. Norwood and K. Jones, Relaxation effects and the measurement of scalar coupling-constants using the Ecosy experiment, *J. Magn. Reson. Ser. A* **104,** 106–110 (1993).

38. A. Kumar, R. C. R. Grace, and P. K. Madhu, Cross-correlations in NMR, *Prog. Nucl. Magn. Reson. Spectrosc.* **37,** 191–319 (2000).

39. I. Bertini, C. Luchinat, and D. Tarchi, Are true scalar proton–proton connectivities ever measured in cosy spectra of paramagnetic macromolecules, *Chem. Phys. Lett.* **203,** 445–449 (1993).

40. J. Qin, F. Delaglio, G. N. Lamar, and A. Bax, Distinguishing the effects of cross-correlation and J-coupling in Cosy spectra of paramagnetic proteins, *J. Magn. Reson. Ser. B* **102,** 332–336 (1993).

41. G. S. Harbison, Interference between J-couplings and cross-relaxation in solution NMR-spectroscopy—Consequences for macromolecular structure determination, *J. Am. Chem. Soc.* **115,** 3026–3027 (1993).

42. M. Billeter, D. Neri, G. Otting, Y. Q. Qian, and K. Wuthrich, Precise vicinal coupling-constants 3J(HN-HA) in proteins from nonlinear fits of J-modulated [15N,1H]-COSY experiments, *J. Biomol. NMR* **2,** 257–274 (1992).

43. H. Kuboniwa, S. Grzesiek, F. Delaglio, and A. Bax, Measurement of HN-Ha J-couplings in calcium-free calmodulin using new 2D and 3D water-flip-back methods, *J. Biomol. NMR* **4,** 871–878 (1994).

44. A. Bax and L. Lerner, Measurement of ^{1}H–^{1}H coupling constants in DNA fragments by 2D NMR, *J. Magn. Reson.* **79,** 429–438 (1988).

45. J. Yang, K. McAteer, L. A. Silks, R. Wu, N. G. Isern, C. J. Unkefer, and M. A. Kennedy, A comprehensive approach for accurate measurement of proton–proton coupling constants in the sugar ring of DNA, *J. Magn. Reson.* **146,** 260–276 (2000).

46. A. Bax, G. W. Vuister, S. Grzesiek, F. Delaglio, A. C. Wang, R. Tschudin, and G. Zhu, Measurement of homonuclear and heteronuclear J-couplings from quantitative J-correlation, *Meth. Enzymol.* **239,** 79–105 (1994).

47. G. Otting, M. Ruckert, M. H. Levitt, and A. Moshref, NMR experiments for the sign determination of homonuclear scalar and residual dipolar couplings, *J. Biomol. NMR* **16,** 343–346 (2000).

48. W. Peti and C. Griesinger, Measurement of magnitude and sign of H, H-dipolar couplings in proteins, *J. Am. Chem. Soc.* **122,** 3975–3976 (2000).